

Amorphous silica and its effects on shale reservoir: A case study about Yanchang formation lacustrine shale, Ordos Basin

Guoheng Liu, Gangyi Zhai, Caineng Zou, Zhilong Huang, Bo Liu, Xiaobo Guo, Tianxu Guo, Mingrui Chai & Hao Wang

To cite this article: Guoheng Liu, Gangyi Zhai, Caineng Zou, Zhilong Huang, Bo Liu, Xiaobo Guo, Tianxu Guo, Mingrui Chai & Hao Wang (2018): Amorphous silica and its effects on shale reservoir: A case study about Yanchang formation lacustrine shale, Ordos Basin, Energy Sources, Part A: Recovery, Utilization, and Environmental Effects, DOI: [10.1080/15567036.2018.1522395](https://doi.org/10.1080/15567036.2018.1522395)

To link to this article: <https://doi.org/10.1080/15567036.2018.1522395>



Published online: 19 Sep 2018.



Submit your article to this journal [↗](#)



View Crossmark data [↗](#)



Amorphous silica and its effects on shale reservoir: A case study about Yanchang formation lacustrine shale, Ordos Basin

Guoheng Liu^{a,b}, Gangyi Zhai^a, Caineng Zou^c, Zhilong Huang^b, Bo Liu^d, Xiaobo Guo^e, Tianxu Guo^a, Mingrui Chai^f, and Hao Wang^g

^aOil and Gas Survey, China Geological Survey, Beijing, China; ^bState Key Laboratory of Petroleum Resources and Prospecting, China University of Petroleum, Beijing, China; ^cResearch Institute of Petroleum Exploration and Development, PetroChina, Beijing, China; ^dAccumulation and Development of Unconventional Oil and Gas, State Key Laboratory Cultivation Base Jointly-constructed by Heilongjiang Province and Ministry of Science and Technology, Northeast Petroleum University, Daqing, China; ^eSchool of Earth Sciences and Engineering, Xi'AN University of Petroleum, Xi'An, China; ^fCollege of Earth Science, Yangtze University, Wuhan, Hubei, China; ^gSchool of Earth Sciences and Resources, China University of Geoscience, Beijing, China

ABSTRACT

The content of amorphous silica in Yanchang formation shale ranges from 1.48% to 19.89%, with an average of 11.77%. The Chang 7–3 submember (the submember 3 of the seventh member of Upper Triassic Yanchang formation) shale contains much larger content of amorphous silica. Amorphous silica appears as opal rim closely adjacent to detrital quartz, cement among clay minerals, and cement aside detrital minerals. Silica originates from clay mineral transformation and pressure solution of detrital quartz. Mineral composition, growth space, and overpressure affect the content of amorphous silica. Amorphous silica reduces the brittleness of shale reservoir, decreases the density of Chang 7–3 submember shale, and causes an increase in AC values for Chang 7–3 submember shale.

ARTICLE HISTORY

Received 2 August 2018
Revised 25 August 2018
Accepted 6 September 2018

KEYWORDS

Amorphous SiO₂; lacustrine shale; ordos basin; QEMSCAN; quantitative calculation

Introduction

Mineral composition is usually the foundation in all researches about shale reservoir. Most shale mainly consists of clay and detrital minerals, such as Yanchang formation shale in Ordos Basin, Lower Cambrian shale, and Wufeng-Longmaxi-Niutitang Formation shale in Sichuan Basin (Han et al. 2013; Jiang et al. 2016; Lai et al. 2015; Luo et al. 2017). Some other productive shale contains a high concentration of siliceous minerals, limestone, and minor dolomite, such as the Barnett shale (Ross and Bustin 2008). Moreover, there are shale reservoirs, such as Niobrara Formation shale and the lower black mud rock member of the Besa River, Colorado, which are dominated by calcite and clay minerals (Kuila et al. 2012; Ross and Bustin 2008). Some shale even develops tuffaceous matter, such as Permian Lucaogou Formation shale in Santanghu Basin, China (Liu et al. 2015). Researchers discussed the great effect of mineral on shale reservoir properties, such as shale brittleness, shale pore space, microfracture development, and gas-bearing property, based on the research of mineral composition (Jarvie et al. 2007; Kuila et al. 2012; Ross and Bustin 2008; Zou et al. 2010).

In previous researches, X-ray diffraction (XRD) and X-ray fluorescence (XRF) are commonly used to evaluate the mineral composition and elemental composition in shale reservoirs. XRD cannot quantitatively calculate all the constituent parts in shale, such as amorphous silica, because amorphous silica cannot display diffraction properties of the crystal. XRF (XRF) also cannot indicate the mineral composition

CONTACT Bo Liu  liuguoheng123@yeah.net; Xiaobo Guo  xygcup1989@sina.com

Guoheng Liu, Gangyi Zhai, Caineng Zou and Zhilong Huang are Equally contributors

Color versions of one or more of the figures in the article can be found online at www.tandfonline.com/ueso.

because this method is used for elemental analysis. But, amorphous silica is surely developed in shale and also has a significant impact on the physical properties of shale reservoir.

There are some studies that focused on amorphous silica and qualitatively described the effect of amorphous silica on physical properties of the shale reservoir. The amorphous silica in marine and lacustrine shale is mainly originated from sponge spicules, such as the Monterey Formation shale and shale in the Liard Basin, and smectite–illite transformation and pressure solution of detrital quartz, respectively (Peltonen et al. 2009; Ross and Bustin 2008; Thyberg et al. 2010). The amorphous silica induced great changes for physical properties of shale reservoir. After undergoing diagenesis to opal-CT, which was made up of tiny microcrystalline blades with water content as high as 10 wt%, porosity typically drops from around 45% to below 25%, permeability drops to negligible levels, and the rock becomes well-indurated and brittle (Chaika and Williams 2001). The effect of amorphous silica on shale reservoir can also be reflected by the changes in acoustic travel time logging and density logging responses (Peltonen et al. 2009; Thyberg et al. 2010).

However, qualitative description rather than quantitative analysis was conducted in all of these researches. This study quantitatively analyzed the content of amorphous silica. On the basis of quantitative calculation of amorphous silica in shale, the controls to amorphous silica formation and the effects of amorphous silica on shale reservoir property were also discussed.

Geological setting

The Ordos Basin is an important and major petroliferous basin situated in the central part of the North China (Figure 1). It is a multicycle cratonic basin developed on the Archean granulites and lower Proterozoic greenschists of the North China Block (Yang, Zhang, and Tang 2013; Lai

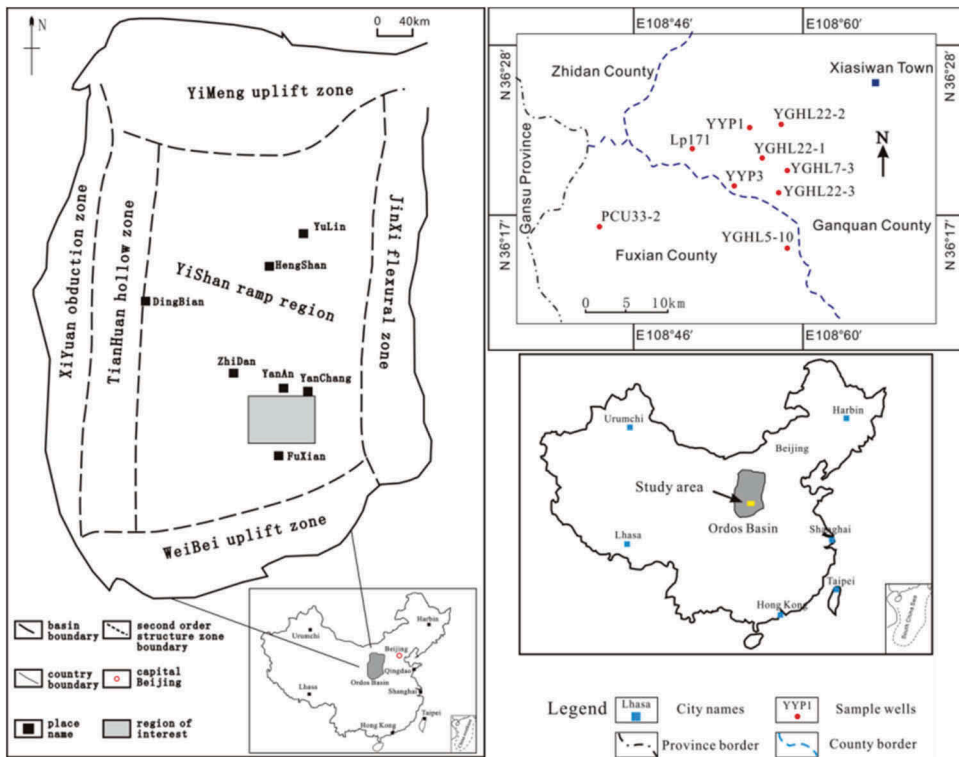


Figure 1. Map of the research area in the Ordos Basin, central China.

et al. 2016). The Ordos Basin can be divided into six tectonic units. The research area is located in the southeast of the Yishan ramp region. The Yanchang formation shale layers were deposited in a freshwater lacustrine sedimentary environment, contains significant organic matter, lamina, pyrite framboids, and nano-fossils (Chen and Li 2007). The late Triassic Yanchang formation has been divided into 10 members according to the marker beds and sedimentary cycles. Shale layers, the main source rock in the area, are primarily deposited in Chang 7 member (C7M). Shale of Chang 7 member can be divided into Chang 7-2 submember (C7-2SM) and Chang 7-3 submember (C7-3SM), both of which display higher gamma readings at the upper parts (Figure 2) because of containing volcanic debris with radioactive substances (Qiu et al. 2011). Yanchang formation shale layers include black shale, oil shale, dark gray mudstone, and silty mudstone (Figure 3). The two submembers show significant differences in their acoustic time

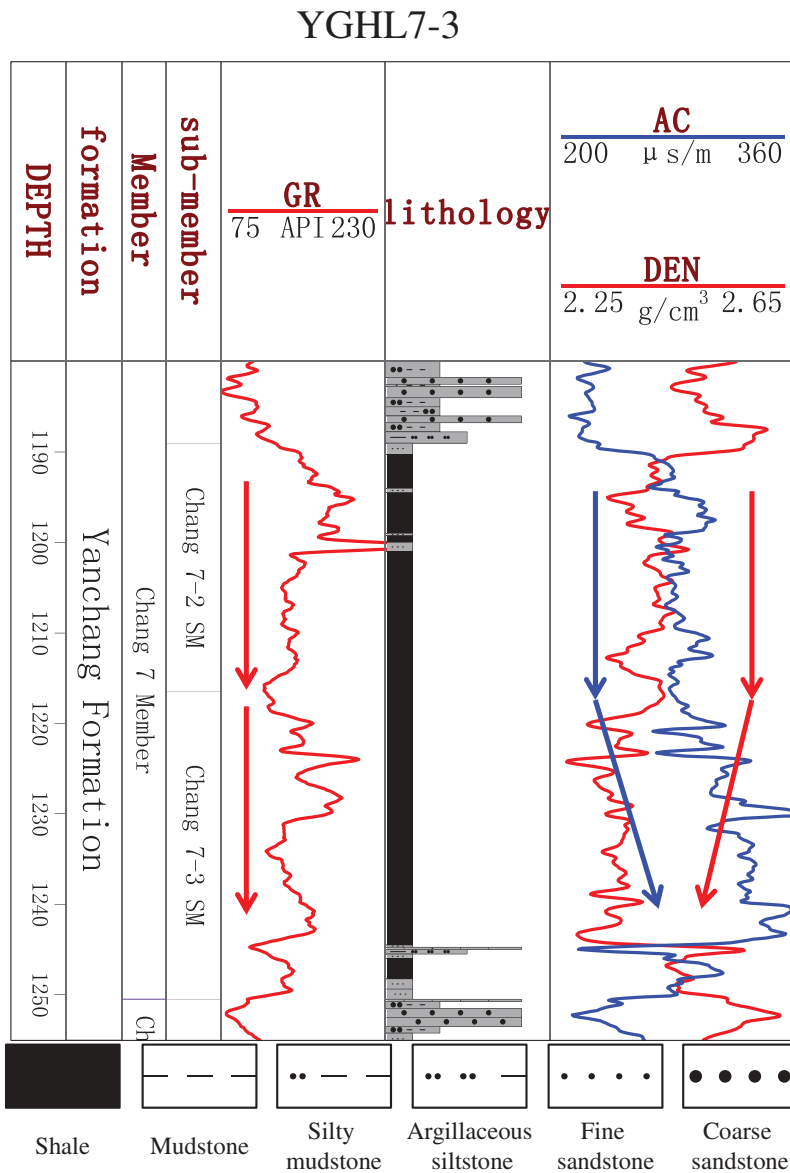


Figure 2. Lithological and logging characteristics of Chang 7 member shale in the Ordos Basin.



Figure 3. Core photos of the Yanchang formation shale reservoir.

A: YGHL7-3, 1,190.5 m, Black shale; B: PCU33-2, 1,645.35 m, oil shale; C: YYP3, 1,198.85 m, dark gray mudstone; D: LP171, 1,509.85 m, silty mudstone

and density data, with C7-3SM displaying abrupt increase in sonic transit time (AC) values and decrease in bulk density (DEN) values (Figure 2).

Material and methods

Material

A total of 30 prospecting wells within the Odors Basin have penetrated the bottom of the Yanchang formation to date. In this study, more than 300 samples were obtained from nine of these wells (Figure 1) for use in experimental analyses. Samples were freshly cut after removing the weathered surface of the core. Shale and mudstone samples were used in all the analysis except scanning electron microscope (SEM) observation, in which silty mudstone samples were used.

Methods

Geochemical analysis

Rock-Eval pyrolysis is an established method for the geochemical characteristic of sedimentary rocks. The samples were subjected to programmed heating in an inert atmosphere to determine the amount of volatile gas and residual hydrocarbons (S_1 peak) and the amounts of nonvolatile hydrocarbons and oxygen-containing organic compounds released during thermal cracking of the remaining organic matter in the rock (recorded as S_2).

Lithology analysis

The samples from Yanchang formation shale were ground to powder finer than $2\ \mu\text{m}$ and analyzed for whole-bulk and clay fraction mineralogy by quantitative XRD. The mineral composition was measured by a Rigaku automated powder diffractometer (D/MAX-RA) equipped with a Cu X-ray source (40 kV, 35 mA). The bulk mineral composition of the powder sample was determined over an angular range of 4 to $70^\circ 2\theta$ at a scanning speed of $1^\circ 2\theta/\text{min}$. The different clay minerals were determined over an angular range of 3 to $65^\circ 2\theta$ at a scanning speed of $1.5^\circ 2\theta/\text{min}$. Quantification of the minerals was based on calculations of the integrated area of the clay minerals using Jade 6.5 software.

Porosity and permeability analysis

The porosity of dry samples was determined by grain density obtained from helium pycnometry and bulk volume of the plugs was calculated from mercury immersion (Chalmers et al., 2011; Cui, Bustin, and Bustin 2009). The total porosity was calculated from the difference between bulk and skeletal densities. The permeability was calculated from measurements with helium expansion at a constant temperature of 30°C and a range of pressures from 5 MPa to 30 MPa in a stepwise increase (Ghanizadeh et al. 2014).

Mechanical properties of rock tests

The core samples had a diameter of 25 mm and a length-to-diameter ratio of 2. The stress was loaded until the sample was irrevocably damaged. Rock mechanical parameters, including compressive strength, Young's modulus, and Poisson's ratio, were tested by GCTS-RTR-1500 (Geotechnical Consulting and Testing Systems, Rapid Triaxial Rock Testing System) under constant confining pressure (10 MPa) conditions. The confined pressure limit of the equipment was 210 MPa; the capacity of the axial loading was 1,500 kN; the radial and axial displacement limits were ± 2.5 mm, respectively. The samples in this research had no factitious fractures on the surface formed during the drilling process.

Pore image analysis

Image analysis in this research was conducted on a SEM equipped with an energy-dispersive spectrometer (EDS). Fresh plane of fracture is used in this study. The surface of the fresh plane was coated with Au to improve acquisition of secondary as well as EDS data. SEM analyses were undertaken after coating the samples with Au at an operating current of 15kV.

QEMSCAN analysis

The QEMSCAN is a high-throughput automated analysis solution, used mainly in the natural resources industry, where analysis of particulates is required to solve practical problems or to improve scientific processes. The system comprises a SEM with a large specimen chamber, multiple high-speed EDSs, and state-of-the-art automated quantitative mineralogy image analysis and microanalysis software.

Quantitative analysis of amorphous SiO_2

The content of quartz acquired by QEMSCAN should include the content of crystalline state quartz and amorphous silica because the minerals were identified according to elemental composition determined by EDS (Figure 4). The content of quartz can be calculated by XRD. Then, the content of amorphous silica can be calculated by combining XRD and QEMSCAN. The calculation formula and process have been described in detail by Huang et al. (2015).

Results

Composition characteristics

S_1 for C7-2SM shale varies from 1.35 mg/g to 6.61 mg/g, with a mean of 3.63 mg/g, while S_1 for C7-3SM shale ranges from 3.71 mg/g to 10.87 mg/g (Figure 5). S_2 for C7-2SM shale ranges from 3.75 mg/g to 15.43 mg/g with an average of 8.03 mg/g, while S_2 for C7-3SM shale varies from



Figure 4. The QEMSCAN of shale sample from Yanchang formation of Ordos Basin.

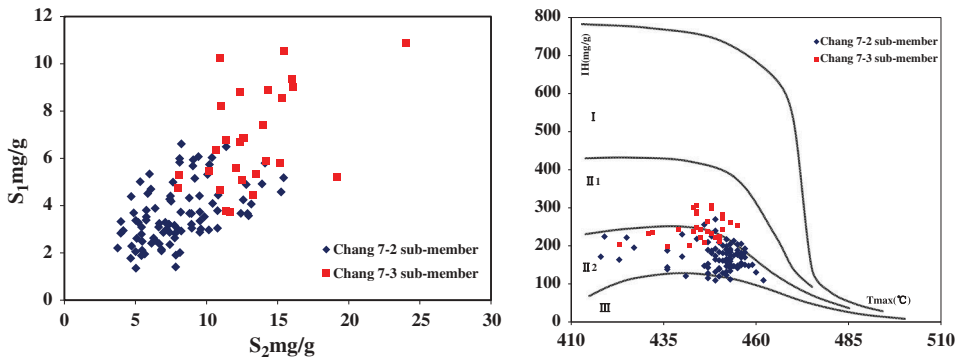


Figure 5. Relationships between S_1 and S_2 and plot of the hydrogen index (HI) versus T_{max} .

8.02 mg/g to 24.05 mg/g with an average of 13.19 mg/g (Figure 5). The values of S_1 and S_2 for C7-3SM shale samples are larger, which means C7-3SM shale samples contain larger content of residual hydrocarbon and kerogen. The kerogen in C7-2SM shale mainly contains Type II₂ and possibly Type III organic matter. Approximately half of the C7-3SM shale samples contain Type II₁ organic matter and the other half Type II₂ (Figure 5).

The content of clay minerals and detrital minerals are approximately equal. Quartz and an illite–smectite mixed layer are the major components of detrital and clay minerals, respectively. The amounts of different types of clay and detrital minerals do not vary greatly between C7-2SM and C7-3SM (Figure 6). C7-3SM displays larger content of the illite–smectite mixed layer (66.95%) and reducing minerals (9.26%), but lower content of quartz (25.42%).

The volume percentage of quartz and amorphous silica in C7-3SM shale varies from 40.07% to 49.75%, with a mean of 46.803%, while that in C7-2SM shale ranges from 34.03% to 43.25%, with a mean of 39.592% (Table 1). The content of amorphous silica (mass of percentage) in Yanchang formation shale ranges from 1.48% to 19.89%, with an average of 11.77% (Table 1). The average content of amorphous silica in C7-3SM shale is 16.25%, while that in C7-2SM shale is 7.29%. C7-3SM shale contains a larger content of amorphous silica than that of C7-2SM shale (Figure 6).

Porosity characteristics

Yanchang formation shale displays apparently low porosity and permeability. Porosity ranges from 0.162% to 2.69%, with an average of 1.57%. Permeability varies from 0.000047 mD to 0.007 mD, with a mean of 0.0012 mD. There is no huge difference in porosity and permeability between C7-2SM shale samples and C7-3SM shale samples (Figure 7). Much more researches about porosity and pore structure were presented in Lai et al. (2018).

Mechanical properties of rock

Young's modulus of Yanchang formation shale ranges from 13.3 N/mm² to 71.4 N/mm², with an average of 36.5 N/mm². Poisson's ratio of Yanchang formation shale ranges from 0.202 to 0.406, with an average of 0.31. Samples of C7-3SM shale exhibit lower values of Young's modulus and Poisson's ratio than samples of C7-2SM shale (Table 2)

SEM observation

Authigenic quartz mainly occurred in pores with diameters about 5 ~ 30 μm and isolated by clay minerals (Figure 8). These pores are usually filled with authigenic quartz, chlorite, and dolomite.

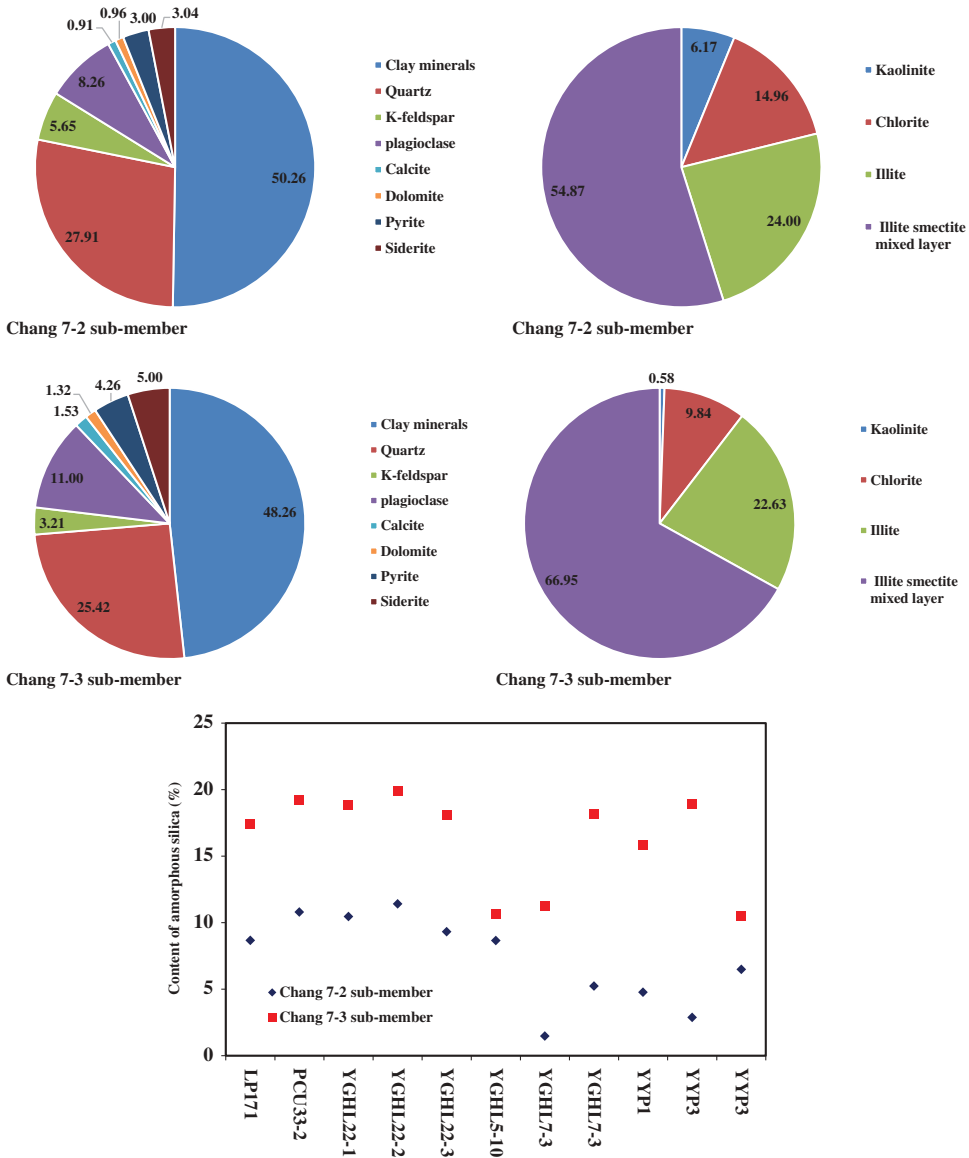


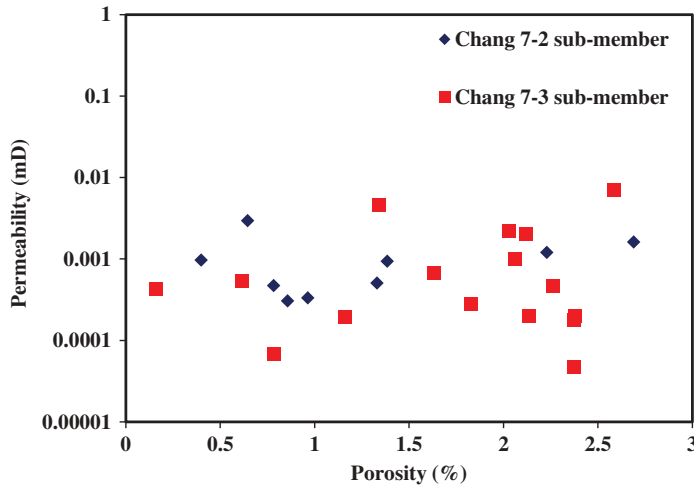
Figure 6. Mineral composition of Yanchang formation shale samples.

Authigenic chlorite and dolomite can be clearly observed in pores developed in silty mudstone (Figure 8d–i). Authigenic quartz is usually less than 10 μm in diameter and emerges among authigenic chlorite particles. Dolomite is located in the center of these pores (Figure 8d–f), and chlorite nearest to the rim, leaving quartz occurred between them. The phenomenon that quartz crystals live together with dolomite indicates a change of pore fluid in pH.

Detrital quartz is easily observed, especially in silty mudstone samples. They are usually surrounded by clay minerals or amorphous silica (Figure 9). Rims of detrital quartz are always jagged, indicating chemical solution (Figure 9a,b). Amorphous silica in Yanchang formation shale can be classified into three types. Type I is appearing closely adjacent to detrital quartz as opal rim, which can be distinguished from detrital quartz via different gray level. There is no clear boundary between detrital quartz and this type of amorphous silica. This type of amorphous silica is like micromonticules or granular crystals on

Table 1. Experimental data statistics of the method to calculate amorphous silica.

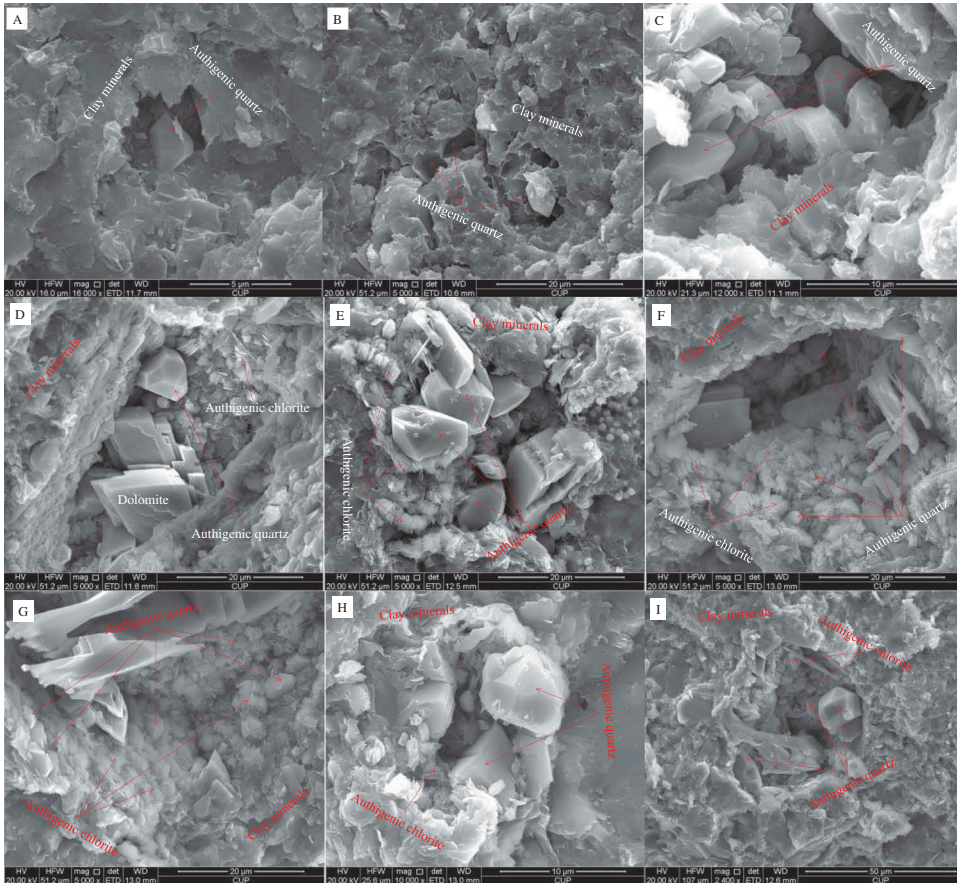
Sample ID	Depth (m)	Member	Mass percentage of quartz (%)	Average density of amorphous silica (g/cm ³)	Average density of quartz (g/cm ³)	Density of sample (g/cm ³)	Volume percentage of silica mineral (%)	Mass percentage of amorphous silica (%)
LP171	1,509.25	C7-2SM	34	2.19	2.5915	2.49	39.592	8.67
PCU33-2	1,619.32	C7-2SM	35	2.19	2.5915	2.55	43.13	10.79
YGHL22-1	1,146.97	C7-2SM	32	2.19	2.5915	2.53	39.91	10.46
YGHL22-2	1,205.45	C7-2SM	34	2.19	2.5915	2.58	43.25	11.41
YGHL22-3	1,446.75	C7-2SM	36	2.19	2.5915	2.51	42.18	9.32
PCU33-2	1,614.42	C7-2SM	35	2.19	2.5915	2.61	42.41	8.66
YGHL7-3	1,189.85	C7-2SM	34	2.19	2.5915	2.62	35.63	1.48
YGHL7-3	1,196.35	C7-2SM	37	2.19	2.5915	2.57	40.87	5.23
YYP1	1,421.9	C7-2SM	30	2.19	2.5915	2.58	34.03	4.77
YYP3	1,200.1	C7-2SM	32	2.19	2.5915	2.57	34.19	2.88
YYP3	1,199.4	C7-2SM	35	2.19	2.5915	2.59	40.32	6.49
LP171	1,554.15	C7-3SM	34	2.19	2.5915	2.51	46.803	17.42
PCU33-2	1,639.6	C7-3SM	35	2.19	2.5915	2.55	49.75	19.20
YGHL22-1	1,189.45	C7-3SM	34	2.19	2.5915	2.53	48.3	18.85
YGHL22-2	1,248.45	C7-3SM	33	2.19	2.5915	2.57	49.11	19.89
YGHL22-3	1,486.75	C7-3SM	35	2.19	2.5915	2.57	49.26	18.08
PCU33-2	1,644.42	C7-3SM	34	2.19	2.5915	2.55	42.15	10.67
YGHL7-3	1,211.15	C7-3SM	32	2.19	2.5915	2.5	40.07	11.24
YGHL7-3	1,216.33	C7-3SM	34	2.19	2.5915	2.57	48.5	18.14
YYP1	1,454.9	C7-3SM	36	2.19	2.5915	2.6	48.85	15.80
YYP3	1,230.1	C7-3SM	34	2.19	2.5915	2.57	49.14	18.94
YYP3	1,231.1	C7-3SM	36	2.19	2.5915	2.5	42.9	10.48

**Figure 7.** Cross-plot of porosity and permeability.

the surface of detrital quartz (Figure 9c–e). Type II is emerging among clay minerals as cement. Most of the amorphous silica among clay minerals usually display no concrete form or shape (Figure 9 F), but occasionally they are sheet like (Figure 9h,j,k). This type of amorphous silica mainly occurs in pure shale. Type III is emerging aside detrital minerals as cement (Figure 9l,n,o). A clear boundary or crack can be observed between this amorphous silica and other minerals. This type of amorphous silica may be from shale around the silty mudstone. Amorphous silica released from smectite to illite or chlorite transformation transported to silty mudstone because of compaction during diagenesis. More details about silica in shale reservoir were presented in Liu et al. (2016).

Table 2. Experimental data statistics of Young's modulus and Poisson's ratio.

Sample ID	Depth (m)	Member	Mass percentage of quartz (%)	Mass percentage of amorphous silica (%)	Young's modulus (N/mm ²)	Poisson's ratio
LP171	1,509.25	C7-2SM	34	8.67	36.8	0.344
PCU33-2	1,614.42	C7-2SM	35	8.66	42.1	0.385
YGHL7-3	1,196.35	C7-2SM	37	5.23	71.4	0.406
YGHL22-2	1,205.45	C7-2SM	34	11.41	34.4	0.401
YGHL22-3	1,446.75	C7-2SM	36	9.32	42.6	0.337
YYP1	1,454.9	C7-3SM	36	15.80	34.2	0.271
YGHL22-2	1,248.45	C7-3SM	33	19.89	13.3	0.202
YGHL22-1	1,189.45	C7-3SM	34	18.85	25.4	0.24
LP171	1,554.15	C7-3SM	34	17.42	28.7	0.204

**Figure 8.** SEM images of authigenic quartz in Yanchang formation shale (Liu et al. 2016). A ~ C: shale; D ~ I: silty mudstone.

Discussion

Origin of silica in shale layers

Clay mineral transformation, such as smectite transforming to chlorite, is one of the original processes of silica in Yanchang formation lacustrine shale. A series of evidence prove that clay mineral transformation has been going on in Yanchang formation shale. First, amorphous silica was

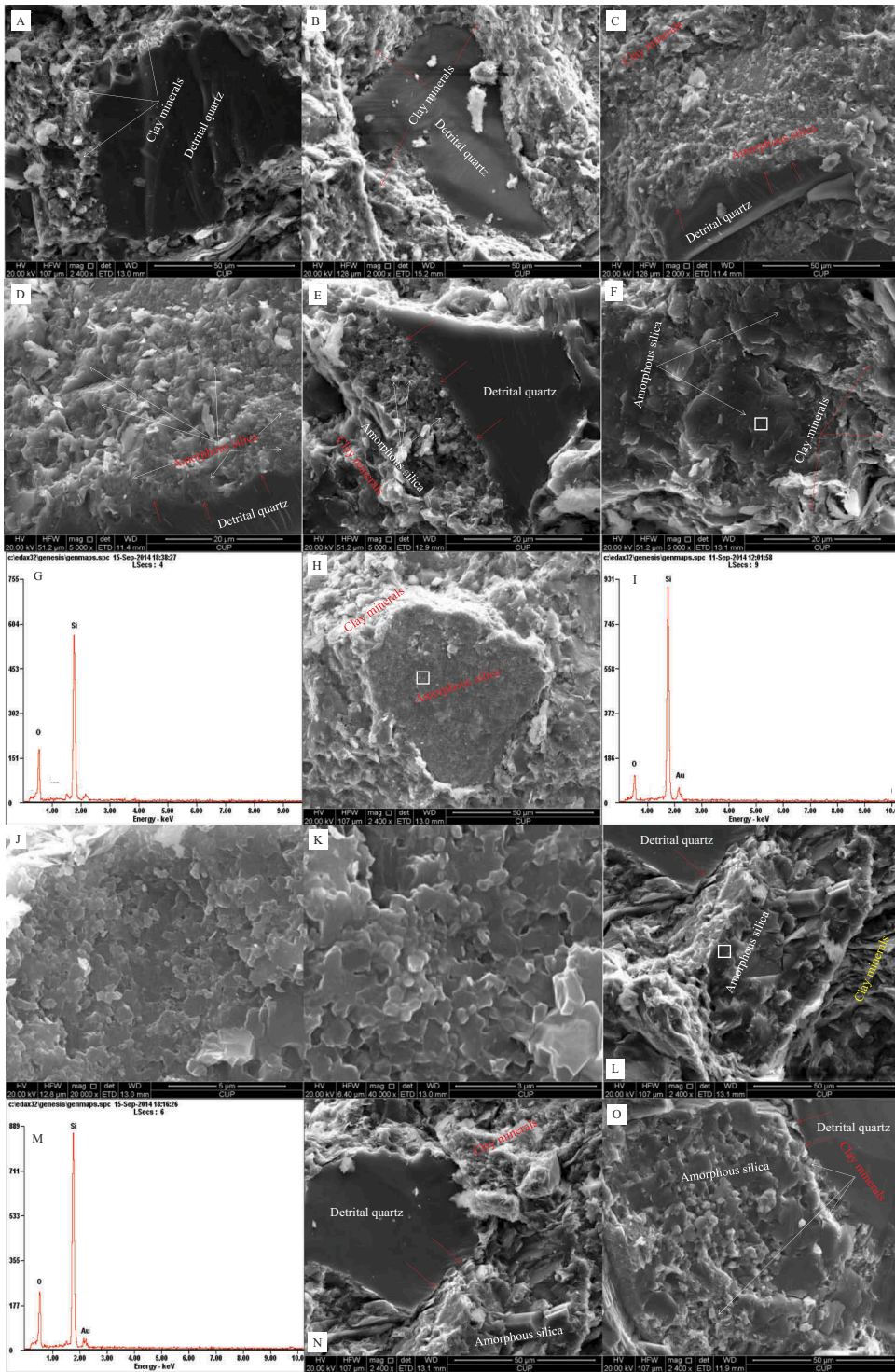


Figure 9. SEM images of detrital quartz and amorphous silica in Yanchang formation shale (Liu et al. 2016). A ~ E: silty mudstone; F ~ K: shale; L ~ O: silty mudstone. The red arrows indicate the boundary between amorphous silica and other minerals.

observed between clay minerals (Figure 9f,h). Second, some small authigenic quartz usually emerges among authigenic chlorite particles.

Pressure solution of detrital quartz is another original process of silica in Yanchang formation lacustrine shale. The jagged or saw-toothed rims of detrital quartz indicate dissolution happened during diagenesis (Figure 9a,b). Large content of amorphous silica is closely adjacent to detrital quartz as overgrowth. This amorphous silica and detrital quartz are tightly surrounded by clay minerals, which do not display the state and morphology like authigenic chlorite. This phenomenon suggests that amorphous silica closely adjacent to detrital quartz is not from clay mineral transformation but detrital quartz dissolution.

Controlling factors of amorphous silica

Composition

Clay mineral transformation and pressure solution of detrital quartz are the original processes of silica. Hence, mineral composition is one factor to amorphous silica. C7-3SM shale displays a larger content of the illite/smectite mixed layer and a lower content of quartz than C7-2SM shale. More illite/smectite mixed layer means more amorphous silica released from clay minerals transformation. Lower content of quartz indicates larger part of quartz has been dissolved.

Another factor that affects amorphous silica is residual hydrocarbon, which can inhibit the growth of authigenic quartz from silica (Li et al. 2010; Marchand et al. 2001). C7-3SM shale contains much more content of kerogen with better kerogen types, which released more hydrocarbon indicated by the larger values of S_1 for C7-3SM shale.

Growth space

Growth space is an important factor of controlling the content of amorphous silica via confining the growth of authigenic quartz. The SEM observation indicates that all the authigenic quartz, no matter in pure shale (Figure 8a–c) or silty mudstone (Figure 8d–i), is merely formed in relatively large pores. Silica without space around has to stay in an amorphous state (Figure 8). Chang 7 member shale, both C7-2SM shale and C7-3SM shale, displays fairly low porosity (Figure 7), caused by a large content of clay minerals. Clay mineral transformation processes released a large quantity of silica, which cemented mineral particles together and induced lower porosity of shale reservoir. Then, in turn, lacking space stopped amorphous silica from growing into authigenic quartz (Figure 9). Moreover, silica released by pressure solution of detrital quartz are tightly surrounded by clay minerals (Figure 9a,c,e), leaving no space for authigenic quartz growth.

Moreover, pores in pure shale are primarily of nanometer scale size, ranging from less than 10 nm to 100 nm (Nelson 2009; Yang et al. 2013), while authigenic quartz mainly occurred in isolated pores with diameters no less than 5 μm according to SEM observation and statistics. Deficient pore size is another aspect of lacking growth space for authigenic quartz.

Overpressure

Overpressure is another important factor in controlling the content of amorphous silica via confining the growth of authigenic quartz. Overpressure can stop amorphous silica from altering to quartz (Meng et al. 2013; Taylor et al. 2010). A concise description of overpressure is that the liquid was preserved in the pores and bore part of pressure produced by the overlying strata, leaving the mudstone layer undercompacted. Acoustic travel time logging is a useful method to indicate the overpressure in shale. It shows in Figure 10 that AC data of wells increase obviously and abruptly, which means overpressure develops.

Higher content of residual hydrocarbon is an appropriate explanation for the overpressure. Better kerogen types for oil generation cause higher content of residual hydrocarbon in C7-3SM shale. Residual hydrocarbon contained in C7M shale cannot be released out and bear part of pressure, causing the strata not compacted enough.

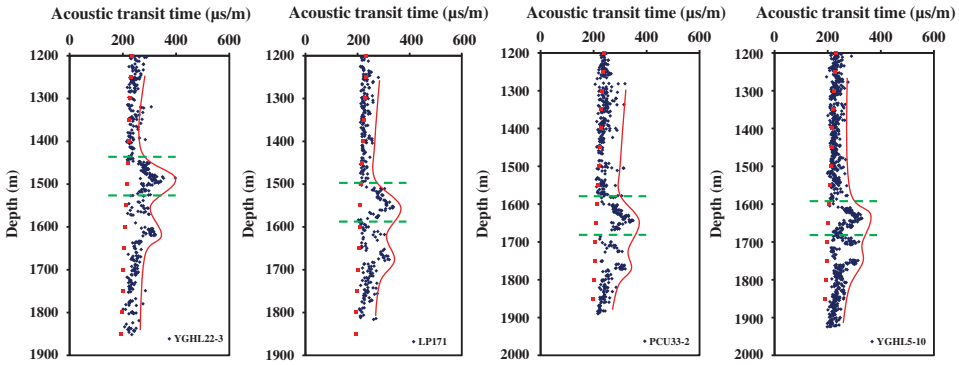


Figure 10. Profiles of sonic transit times versus depth for shale and mudstone.

The dotted red line indicates mudstone normal compaction disciplinary. The solid red line indicates undercompaction disciplinary. The green dotted red lines show the undercompaction zones. Except for shale and mudstone, other types of rocks and AC data corresponding to these rocks have been eliminated.

Influence of amorphous silica on reservoir

Except decreasing shale reservoir porosity (Figure 7), the more severe impact of amorphous silica on the reservoir is decreasing brittleness of shale reservoir by cementing detrital and clay mineral particles together (Figure 11). Both Young’s modulus and Poisson’s ratio show a negative correlation with amorphous silica. Lower values of Young’s modulus and Poisson’s ratio for C7-3SM shale means larger axial plastic deformation than C7-2SM shale. In other words, a higher content of amorphous silica decreases the brittleness of C7-3SM shale, which means more difficult to be fractured.

Moreover, a larger content of amorphous silica is a factor for the higher AC data values and lower DEN data values for C7-3SM shale. Detrital minerals and clay minerals are not the factors that cause the increase in AC and DEN values for C7-3SM shale. First, although C7-2SM shale samples contain lower content of quartz and higher content of illite/smectite mixed layers, the content of detrital minerals and clay minerals do not differ sharply between C7-2SM shale and C7-3SM shale. Second, although acoustic waves travel much faster in quartz than in illite/smectite mixed layers, the speed of acoustic waves does not vary greatly among different kinds of detrital minerals or different types of clay minerals. Similarly, the density does not differ greatly among different kinds of detrital minerals

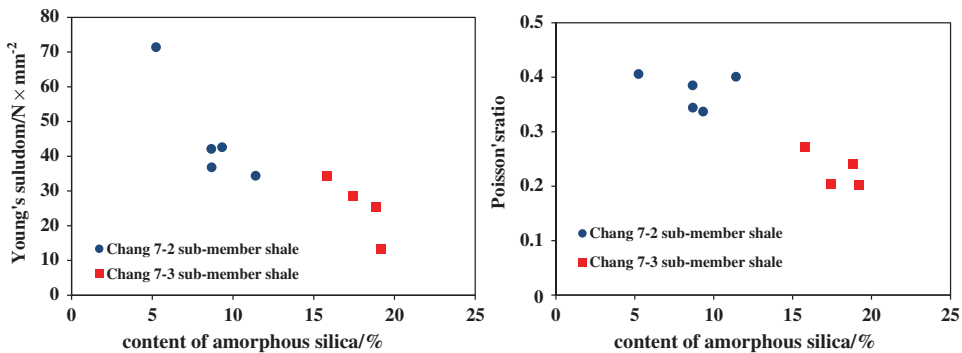


Figure 11. Cross-plot of Young’s modulus, Poisson’s ratio, and content of amorphous silica.

such as quartz and feldspar, or different types of clay minerals. Density of quartz is around 2.65 g/cm^3 . Density of feldspar ranges from $2.61 \text{ g/cm}^3 \sim 2.76 \text{ g/cm}^3$.

Compared with other detrital minerals, such as quartz and feldspar, the density of amorphous silica is much lower. Taking opal as an example, the density of opal is around 2.2 g/cm^3 , while the density of quartz is around 2.65 g/cm^3 . In fact, the density of opal is even much less than that of clay minerals, such as illite and chlorite. The speed of acoustic waves is much faster in minerals or rocks with higher density than that in minerals or rocks with lower density (Buntebarth 1982; Rybach and Buntebarth 1982). More accurately, the average content of amorphous silica in C7-3SM shale is 16.25%, which is larger enough to cause the abrupt increase of AC values for C7-3SM shale. Much larger content of amorphous silica in C7-3SM shale is the key factor to higher AC values and lower DEN values than C7-2SM shale.

Conclusion

- (1) The mass of the percentage of amorphous silica in Yanchang formation shale ranges from 1.48% to 19.89%, with an average of 11.77%. C7-3SM shale contains much larger content of amorphous silica than C7-2SM shale.
- (2) Amorphous silica in Yanchang formation shale can be classified into three types. Type I is appearing closely adjacent to detrital quartz as opal rim. Type II is emerging among clay minerals as cement without concrete form or shape. Type III is emerging aside detrital minerals as cement. Clay mineral transformation and pressure solution of detrital quartz are the original processes of silica in Yanchang formation lacustrine shale. Mineral composition, growth space, and overpressure are the factors controlling the content of amorphous silica via influencing the growth of authigenic quartz.
- (3) Amorphous silica decreases shale reservoir porosity, and reduces the brittleness of shale reservoir. Moreover, a much larger content of amorphous silica decreases the density of C7-3SM shale and causes an increase in AC values for C7-3SM shale.

Funding

Our research was supported by the National Natural Science Foundation of China (No. 41272156 and No. 41472125), the Natural Science Foundation of Shanxi Province, China (2017JQ4004) and the National Science and Technology Major Project of the Ministry of Science and Technology of China (2016ZX05034); the National Natural Science Foundation of China [41272156, 41472125]; the National Science and Technology Major Project of the Ministry of Science and Technology of China [2016ZX05034]; the Natural Science Foundation of Shanxi Province, China [2017JQ4004];

References

- Buntebarth, G. 1982. Density and seismic velocity in relation to mineralogical constitution based on an ionic model for minerals. *Earth and Planetary Science Letters* 57 (2):358–66. doi:10.1016/0012-821X(82)90156-X.
- Chaika, C., and L. A. Williams. 2001. Density and mineralogy variations as a function of porosity in miocene monterey formation oil and gas reservoirs in California. *AAPG Bulletin* 85 (1):149–67.
- Chalmers, G. R., R. M. Bustin, and I. M. Power. 2011. Characterization of gas shale pore systems by porosimetry, pycnometry, surface area, and field emission scanning electron microscopy/transmission electron microscopy image analyses: Examples from the Barnett, Woodford, Haynesville, Marcellus, and Doig units. *AAPG Bulletin* 96:1099–119.
- Chen, Q. H., and W. H. Li. 2007. The deep lacustrine sedimentary and its importance of oil-gas accumulation of Yanchang formation in late triassic of Ordos Basin. *Science China Series D: Earth Science* 37 (1):39–48.
- Cui, X., A. M. Bustin, and R. Bustin. 2009. Measurements of gas permeability and diffusivity of tight reservoir rocks: Different approaches and their applications. *Geofluids* 9:208–23. doi:10.1111/gfl.2009.9.issue-3.
- Ghanizadeh, A., A. Amann-Hildenbrand, M. Gasparik, Y. Gensterblum, B. M. Krooss, and R. Littke. 2014. Experimental study of fluid transport processes in the matrix system of the European organic-rich shales: II. Posidonia Shale (Lower Toarcian, northern Germany). *International Journal of Coal Geology* 123:20–33. doi:10.1016/j.coal.2013.06.009.

- Han, S. B., J. C. Zhang, Y. X. Li, B. Horsfield, X. Tang, W. L. Jiang, and Q. Chen. 2013. Evaluation of lower cambrian shale in Northern Guizhou Province, South China: Implications for shale gas potential. *Energy and Fuels* 27:2933–41. doi:10.1021/ef400141m.
- Huang, Z. L., G. H. Liu, J. Ma, X. Y. Gao, C. C. Chen, C. L. Zhang, Z. Z. Liu, and Z. Y. Chen. 2015. A new method for semi-quantitative analysis of amorphous SiO₂ in terrestrial shale: A case study about Yanchang formation shale, Ordos Basin. *Natural Gas Geoscience* 26 (11):2017–28.
- Jarvie, D. M., R. J. Hill, T. E. Ruble, and R. M. Pollastro. 2007. Unconventional shale-gas systems: The Mississippian barnett shale of north-central Texas as one model for thermo genic shale-gas assessment. *AAPG Bulletin* 91 (4):475–99. doi:10.1306/12190606068.
- Jiang, F. J., D. Chen, J. Chen, Q. W. Li, Y. Liu, X. H. Shao, T. Hu, and J. X. Dai. 2016. Fractal analysis of shale pore structure of continental shale gas reservoir in the Ordos Basin, NW China. *Energy and Fuels* 30 (6):4676–89. doi:10.1021/acs.energyfuels.6b00574.
- Kuila, U., M. Prasad, A. Derkowski, and D. K. McCarty. 2012. Compositional controls on mudrock pore-size distribution: An example from niobrara formation. SPE annual technical conference and exhibition, San Antonio, Texas, USA, October 8–10. SPE-160141-MS.
- Lai, J., G. Wang, Z. Fan, Z. Zhou, J. Chen, and S. Wang. 2018. Fractal analysis of tight shaly sandstones using nuclear magnetic resonance measurements. *AAPG Bulletin* 102 (2):175–93. doi:10.1306/0425171609817007.
- Lai, J., G. Wang, L. Huang, W. Li, Y. Ran, D. Wang, Z. Zhou, and J. Chen. 2015. Brittleness index estimation in a tight shaly sandstone reservoir using well logs. *Journal of Natural Gas Science and Engineering* 27:1536–45. doi:10.1016/j.jngse.2015.10.020.
- Lai, J., G. Wang, Y. Ran, Z. Zhou, and Y. Cui. 2016. Impact of diagenesis on the petrophysical properties of tight oil reservoirs: The case of upper triassic Yanchang formation chang 7 oil layers in ordos Basin, China. *Journal of Petroleum Science and Engineering* 145:54–65. doi:10.1016/j.petrol.2016.03.009.
- Li, R., Y. J. Ge, Y. Chen, Y. Q. Zhou, and H. J. Zhou. 2010. Experimental evidence of influential factor of quartz growth in reservoir. *Journal of China University of Petroleum* 34 (2):13–18.
- Liu, B., Y. F. Lv, Y. L. Meng, X. N. Li, X. B. Guo, Q. Ma, and W. C. Zhao. 2015. Petrologic characteristics and genetic model of lacustrine lamellar fine-grained rock and its significance for shale oil exploration: A case study of permian lucaogou formation in Malang sag, Santanghu Basin, NW China. *Petroleum Exploration and Development* 42 (5):656–66. doi:10.1016/S1876-3804(15)30060-4.
- Liu, G. H., Z. L. Huang, X. B. Guo, Z. Z. Liu, X. Y. Gao, C. C. Chen, and C. L. Zhang. 2016. The research of SiO₂ occurrence in mud shale reservoir of the Yanchang formation in Ordos Basin. *Acta Geologica Sinica* 90 (5):1016–29.
- Luo, Q. Y., J. Y. Hao, C. B. Skovsted, P. Luo, I. Khan, J. Wu, and N. N. Zhong. 2017. The organic petrology of graptolites and maturity assessment of the Wufeng–Longmaxi formations from Chongqing, China: Insights from reflectance cross-plot analysis. *International Journal of Coal Geology* 183:161–73. doi:10.1016/j.coal.2017.09.006.
- Marchand, A. M. E., R. S. Haszeldine, P. C. Smalley, C. I. Macaulay, and A. E. Fallick. 2001. Evidence for reduced quartz-cementation rates in oil-filled sandstones. *Geology* 29 (10):915–18. doi:10.1130/0091-7613(2001)029<0915:EFRQCR>2.0.CO;2.
- Meng, Y. L., C. Xu, H. Y. Xie, W. Z. Tian, C. X. Tong, J. H. Liu, Y. T. Gao, and Y. C. Wang. 2013. A new kinetic model for authigenic quartz formation under overpressure. *Petroleum Exploration and Development* 40 (6):751–57. doi:10.1016/S1876-3804(13)60100-7.
- Nelson, P. H. 2009. Pore-throat sizes in sandstones, tight sandstones, and shales. *AAPG Bulletin* 93 (3):329–40. doi:10.1306/10240808059.
- Peltonen, C., Ø. Marcussen, K. Bjørlykke, and J. Jahren. 2009. Clay mineral diagenesis and quartz cementation in mudstones: The effects of smectite to illite reaction on rock properties. *Marine and Petroleum Geology* 26 (6):887–98. doi:10.1016/j.marpetgeo.2008.01.021.
- Qiu, X. W., C. Y. Liu, G. Z. Mao, and B. L. Wu. 2011. Petrological-geochemical characteristics of volcanic ash sediments in Yanchang formation in Ordos Basin. *Earth Science—Journal of China University of Geosciences* 36 (1):139–50.
- Ross, D. J. K., and R. M. Bustin. 2008. Characterizing the shale gas resource potential of devonian-Mississippian strata in the Western Canada sedimentary basin: Application of an integrated formation evaluation. *AAPG Bulletin* 92 (1):87–125. doi:10.1306/09040707048.
- Rybach, L., and G. Buntebarth. 1982. Relationships between the petrophysical properties density, seismic velocity, heat generation, and mineralogical constitution. *Earth and Planetary Science Letters* 57 (2):367–76. doi:10.1016/0012-821X(82)90157-1.
- Taylor, T. R., M. R. Giles, L. A. Hathorn, T. N. Diggs, N. R. Braunsdorf, G. V. Birbiglia, M. G. Kittridge, C. I. Macaulay, and I. S. Espejo. 2010. Sandstone diagenesis and reservoir quality prediction: Models, myths, and reality. *AAPG Bulletin* 94 (8):1093–132. doi:10.1306/04211009123.
- Thyberg, B., J. Jahren, T. Winje, K. Bjørlykke, J. I. Faleide, and Ø. Marcussen. 2010. Quartz cementation in late cretaceous mudstones, northern North Sea: Changes in rock properties due to dissolution of smectite and precipitation of microquartz crystals. *Marine and Petroleum Geology* 27:1752–64. doi:10.1016/j.marpetgeo.2009.07.005.

- Yang, C., J. C. Zhang, and X. Tang. 2013. Microscopic pore types and its impact on the storage and permeability of continental shale gas, Ordos Basin. *Earth Science Frontiers* 20 (4):240–50.
- Yang, M. H., L. Li, J. Zhou, X. Y. Qu, and D. Zhou. 2013. Segmentation and inversion of the Hangjinqi fault zone, the northern Ordos Basin (North China). *Journal of Asian Earth Sciences* 70-71:64–78. doi:10.1016/j.jseas.2013.03.004.
- Zou, C. N., D. Z. Dong, S. J. Wang, J. Z. Li, X. J. Li, Y. M. Wang, D. H. Li, and K. M. Cheng. 2010. Geological characteristics and resource potential of shale gas in China. *Petroleum Exploration and Development* 37 (6):641–53. doi:10.1016/S1876-3804(11)60001-3.